Acta Materialia 131 (2017) 77–87

Contents lists available at ScienceDirect

Acta Materialia

journal homepage: www.elsevier.com/locate/actamat

Full length article

Creep behavior of submicron copper films under irradiation

P. Lapouge [a], F. Onimus [a, *], M. Coulombier [b], J.-P. Raskin [c, d], T. Pardoen [b, d], Y. Bréchet [e]

[a] Service de recherches Métallurgiques Appliquées, CEA, Université Paris-Saclay, 91191, Gif-sur-Yvette, France
[b] Institute of Mechanics, Materials and Civil Engineering, Université catholique de Louvain, 1348, Louvain-la-Neuve, Belgium
[c] Institute of Information and Communication Technologies, Electronics and Applied Mathematics, Université catholique de Louvain, 1348, Louvain-la-Neuve, Belgium
[d] Research Center in Micro and Nanoscopic Materials and Electronic Devices, Université catholique de Louvain, 1348, Louvain-la-Neuve, Belgium
[e] CNRS SIMAP/Univ. Grenoble Alpes, F-3800, Grenoble, France

ARTICLE INFO

Article history:
Received 20 February 2017
Received in revised form
21 March 2017
Accepted 23 March 2017
Available online 5 April 2017

Keywords:
Irradiation creep
On chip
Thin film
Copper
Deformation mechanism

ABSTRACT

The creep behavior under heavy ion irradiation of 200 nm and 500 nm thick annealed Cu films is characterized using on chip uniaxial microtensile test structures. The tests are performed at room temperature with an applied stress between 100 and 250 MPa and a damage rate of 5×10^{-4} and 6.3×10^{-4} dpa s^{-1}. The deformation rates produced under irradiation are several orders of magnitude larger than when measured out of flux. The main advantage of this method is that it allows the simultaneous measurement of several tens of specimens fully irradiated over their entire thickness. The plasticity mechanisms appear remarkably more homogeneous during irradiation creep than under static loading. The creep power law involves a stress exponent equal to 5 depending only weakly on the microstructure of the films. The SEM and TEM microstructural observations suggest that the creep mechanism results from climb-assisted glide of dislocations as rationalized by a simple closed-form model.

1. Introduction

The understanding of microstructural and mechanical changes under irradiation is of utmost importance for the selection, development and long term assessment of structural materials in the nuclear industry. Irradiation effects are complex, varying from microstructural modifications, involving, among others, formation of point defect clusters and segregation, to the enhancement or emergence of physical phenomena absent in non-irradiated conditions such as swelling, growth or irradiation creep. Among all these phenomena, irradiation creep is a particularly complex phenomenon to characterize with quantitative experiments as well as to model based on the underlying physical mechanisms. Nevertheless, progress in this specific area is essential due to its importance in several nuclear applications. For instance, irradiation creep can lead to dimensional instability of cladding tubes and to the decrease of the fastening torque of bolts exposed to a high neutron flux inside the nuclear core.

The discovery of irradiation creep dates back from the 50's [1,2] but the exact underlying mechanism remains highly debated [3–5]. The most commonly reported and discussed mechanisms are the stress induced preferential nucleation of dislocation loops (SIPN) [6], the stress induced preferential absorption of point defects (SIPA) [7], and the glide of dislocations assisted by climb [8]. Depending on the theory, the applied stress could influence the formation energy of the irradiation clusters, the absorption bias of dislocations or even the diffusion coefficient of the point defects. This uncertainty on the determination of the dominant mechanism results from the difficulty to perform experiments inside a nuclear reactor and to characterize *in situ* the deformation mechanisms.

In experimental reactors, the irradiation creep behavior is usually assessed using stress relaxation tests on metallic strips [9,10] or on pressurized tubes [11,12]. The large thickness of the irradiated region allows testing almost any materials; however, these experiments are time-consuming and costly, and the matter used remains radioactive after irradiation. Jung et al. [13] and Xu et al. [5] have developed specific apparatus to deform materials under a proton flux, the irradiated thickness being of the order of 100 μm. This allows a considerable reduction of the duration of the experiments. Nonetheless, TEM *in situ* observations of the deformation mechanisms during the experiment are impossible. For this, one

* Corresponding author.
E-mail address: fabien.onimus@cea.fr (F. Onimus).

http://dx.doi.org/10.1016/j.actamat.2017.03.056
1359-6454/

needs the use of heavy ion irradiation which has a higher interaction with the material, leading to a thin irradiated thickness (typically several hundreds of nanometers), and higher damage rates. Furthermore, the matter is not activated by low energy ion irradiation. Irradiation inside a TEM, in order to conduct *in situ* experiments, can be performed in a few advanced facilities such as JANNUS in France [14]. In the last few years, Tai et al. [15] and Özerinç et al. [16] have proposed new devices to fully irradiate submicron thick materials samples with heavy ions. However, these devices require the use of a laser or pressurized gas and are not compatible with TEM experiments.

A novel method has recently been described in Ref. [17] to study the irradiation creep with heavy ions. This method requires short experimental times and is amenable to *in situ* experiments under irradiation in a TEM chamber in order to directly observe the deformation mechanisms under irradiation. This method relies on a MEMS inspired technology to apply mechanical stress on a thin metallic film of submicron thickness that can be fully irradiated with heavy ions [18,19]. This method has been used to investigate the irradiation creep behavior of thin Cu films subjected to Cu ion irradiation at room temperature. The behaviors before and after irradiation are compared. The results are analyzed with support of microscopic characterization and of a physically based model to generate a better understanding of irradiation creep mechanisms in Cu. The limitations of the approach are assessed with a specific focus on the representativeness of the data obtained on thin films with grain size that is considered small compared to bulk samples.

2. Materials and experimental methods

The test samples are made of several sets of elementary uniaxial tensile testing structures directly fabricated on a piece of silicon wafer. A silicon nitride film involving up to 1 GPa internal stress is deposited first and patterned by lithography. Then, the Cu film is deposited and patterned as well. As schematized in Fig. 1, the stress is applied on the metallic specimen by the release of the internal stress present in the silicon nitride actuator film, through the etching of the underneath sacrificial layer. This test configuration allows performing stress relaxation experiments on micrometer wide and tens to hundreds micrometer long specimens. The loading system is thus similar to a spring pulling on the specimen. The applied stress, σ, is related to the total strain in the test specimen ε as

$$\sigma = \frac{S_a}{S} E_a \left(-\varepsilon_a^{mis} - \varepsilon \frac{L}{L_a} \right), \quad (1)$$

with S, S_a, L and L_a respectively the specimen and actuator cross-section and length, E_a the Young's modulus of the actuator, and ε_a^{mis} the mismatch strain of the actuator, see Refs. [20–22]. After release, the specimen keeps deforming under the applied stress which slowly decreases with time. This evolution can be probed in order to characterize the creep/relaxation behavior [23].

The feasibility and the relevance of this method to study the creep behavior under heavy ion irradiation have been demonstrated for thin Cu films tested at room temperature in Ref. [17]. The two key points which had been addressed to extend the method to irradiation creep measurements were: i) to protect the actuator beam from the irradiation in order to prevent from any parasitic stress relaxation in the actuator and ii) to perform several irradiation steps to repeat measurements of the strain and the stress variations before and after irradiation. The deformation under irradiation can then be deduced by subtracting, if necessary, the deformation out of flux from the measured deformation. The same protocol is applied on the samples subjected to irradiation as addressed in the present paper.

The actuator layer made of silicon nitride is deposited by Low Pressure Chemical Vapor Deposition (CVD) on a silicon substrate at a temperature of 790 °C. Its thickness is equal either to 80 nm or 150 nm. With such thicknesses, the mismatch strain is around −0.3% leading to a tensile stress before release on the order of 1 GPa in agreement with earlier works, e.g. Ref. [18]. By assuming that the actuator remains elastic, it also serves as a stress sensor via Eq. (1).

The film specimens are made of Cu films obtained by Physical Vapor Deposition (PVD) electron beam evaporation. The Cu target has a purity of 99.999%. Two thicknesses have been studied: 200 nm and 500 nm. After deposition, the samples are annealed at 150 °C to stabilize the microstructure and to generate larger grain sizes.

Both the actuator and the specimen layers are deposited on a sacrificial layer made of a Plasma Enhanced Chemical Vapor Deposition (PECVD) silicon dioxide which is etched in HF solution to release the elementary test structures. An intermediate layer is required between the actuator and the Cu to promote the adhesion of the Cu. Two kinds of adhesion layers have been used: a discontinuous layer of 0.3 nm thick PVD Ti film, and a 4 nm thick PVD Cr film. Most of the samples involve a Cr layer which withstands the HF etching and leads to the best reproducibility of the results among different specimens. Further information on the design and the process can be found in Refs. [21,23,24].

After the etching of the sacrificial layer and the rinsing of the sample in several isopropanol solution baths, the sample is either dried in a Critical Point Dryer equipment to keep the structures freestanding or in air to force the test structures to stick on the

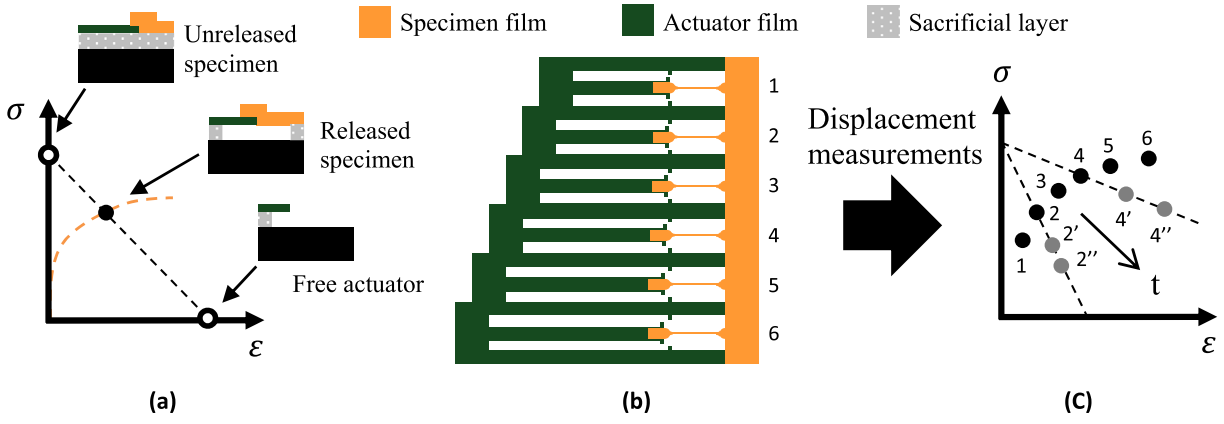

Fig. 1. Basic principle of the method to perform creep/relaxation tests on thin metallic film specimens [17].

substrate. The first method permits the first measurement of the displacement 2 h after the release, while the second method allows a measurement only 15 min after release. However, with the second method the specimens cannot be further deformed by relaxation. Hence, the first method is used to characterize the relaxation behavior of the specimen and the second to study the "instantaneous" strain-stress tensile behavior of the Cu films.

Table 1 summarizes all the sample configurations and experiments conducted in this study. All the specimens exhibit a 6 μm width and every actuators a 15 μm width. The relaxation/creep behavior is determined using a set of test structures in which the specimen length is kept constant and equal to 25, 50, 100 or 400 μm but the actuator length is varied to induce different levels of deformation upon release. The static stress-strain curves are measured with sets of structures involving a constant total length (*i. e.* the sum of specimen and actuator lengths) is kept constant, equal either to 500, 1000 or 2000 μm. On these samples, a specific set of structures with an actuator width of only 1 μm and a specimen width of 15 μm is designed to work under low stress levels. The only exception is for the 200 nm annealed sample which is studied using the same test configuration as the one used for the stress relaxation experiments. A full description of the details of geometrical features of these test structures can be found in Refs. [21,25].

The damage (in dpa or displacement per atom) and damage rate (in dpa/s) in the irradiated specimens is evaluated with the SRIM software by Ziegler [26] using a threshold displacement energy of 25 eV for Cu in the "full damage cascade" mode. The ion energy is selected to be equal to 600 keV for the 200 nm thick specimens and 1200 keV for the 500 nm thick specimens. With these energies, the entire thickness of the two types of sample is fully and almost homogenously irradiated. The damage rates during the irradiation were respectively 5×10^{-4} dpa/s (8×10^{14} ions. m^{-2} s^{-1}) and 6.3×10^{-4} dpa/s (12×10^{14} ions m^{-2} s^{-1}). The damage rates and damage doses indicated in Table 1 correspond to the mean value of the irradiation damage in the film. The damage profiles have been presented in Ref. [17].

The microstructure of the films before and after irradiation has been presented in Ref. [17]. The Cu film exhibits a {111} fiber texture with a grain size which is roughly equal to the thickness of the film in the annealed state. After irradiation at room temperature, the defects mainly consist of a high density (~2.5 10^{23} m^{-3}) of Stacking Fault Tetrahedra (SFT).

3. Results

3.1. Unirradiated copper film

The measurement of the displacement u on the test structures directly provides the total strain of the specimen, $\frac{u}{L_0}$. This total strain is the sum of the mismatch ε^{mis}, due to the internal stress in the test material, and of the mechanical strain ε^{mech}. In the following, the "strain" will always refer to the mechanical strain which is the sum of the elastic, plastic and, if relevant, creep contributions.

Table 2
Internal stress and strain measured by the Stoney method in the copper films.

	σ^{int}	ε^{mis}
200 nm Cu film/Ti clusters, unannealed film	150 MPa	−0.08%
200 nm Cu film/4 nm Cr layer, unannealed film	~0	~0
200 nm Cu film/4 nm Cr layer, annealed film	425 MPa	−0.2%
500 nm Cu film/4 nm Cr layer, unannealed film	~0	~0
500 nm Cu film/4 nm Cr layer, annealed film	285 MPa	−0.15%

The internal stress is measured independently using the Stoney method. The copper films as well as their adhesion layer are deposited on a bare silicon wafer coated with silica. The change of curvature before and after deposition and after annealing gives the internal stress, σ^{int}, from the Stoney formula [27]. The internal stress can then be converted into the corresponding elastic strain with the biaxial modulus $E/(1-\nu)$, where E is the Young's modulus and ν is the Poisson ratio. For a perfect fiber texture {111}, E is equal to 130 GPa in Cu [28] and ν is close to 0.34 [29]. Table 2 gives σ^{int} and ε^{mis} for the different cases. The internal stress of the annealed 200 nm thick sample with an adhesion layer of Ti clusters has not been characterized. In first approximation, we have taken the same value as for the samples with the Cr layer.

Fig. 2 shows the stress-strain curves obtained with the on-chip test structures, up to failure, for the samples indicated in Table 1. As mentioned in the description of the samples, the points corresponding to the first 0.2% of deformation for the 200 nm and 500 nm thick samples are obtained using a specific set of test structures present on both samples. This kind of test structures is not available on the 200 nm thick non annealed film samples.

The behavior of the three films is quite similar up to 1% deformation. The elastic stiffness is smaller than the theoretical value of 130 GPa. Based on the first data points, the elastic modulus of the 500 nm thick film and 200 nm thick film is respectively around 100 and 75 GPa in the annealed state.

The annealed specimens show a lower ductility than the specimen without annealing. Plastic localization occurs in the three specimens within large grains (>1 μm) through intense slip bands, see Fig. 3a, as also reported in Ref. [21]. The rest of the surface of the specimen remains unchanged. The TEM micrograph, shown in Fig. 3b, reveals several dislocation pile-ups parallel to the fracture surface. Plastic deformation is clearly controlled by dislocation glide.

Fig. 4 shows several examples of the variation with time of ε and σ, for the different samples. The evolution of the strain is logarithmic with time for all specimens. The annealed 200 nm thick samples have been monitored for 3700 h while the deformation of the unannealed samples was monitored during 190 h only. The

Table 1
List of samples and experiments. All the experiments have been conducted at room temperature.

Cu film	Adhesion layer	Si_3N_4 thickness	Type of measurements	Irradiation, energy, damage rate (dpa/s)	Irradiation steps, final damage dose
200 nm unannnealed	Ti clusters	85 nm	Stress-Strain curve/Relaxation	Unirradiated	–
200 nm annealed at 150 °C	Ti clusters	85 nm	Stress-Strain curve	Unirradiated	–
200 nm annealed at 150 °C	4 nm Cr film	80 nm	Relaxation/*Post* irradiation relaxation	Unirradiated and irradiated with 600 keV Cu ions at 5×10^{-4} dpa/s	1 step up to 1 dpa before release
500 nm annealed at 150 °C	4 nm Cr film	150 nm	Stress-Strain curve	Unirradiated	–
500 nm annealed at 150 °C	4 nm Cr film	85 nm	Relaxation/Irradiation creep	Unirradiated and irradiated with 1200 keV Cu ions at 6.3×10^{-4} dpa/s	5 steps up to 8 dpa

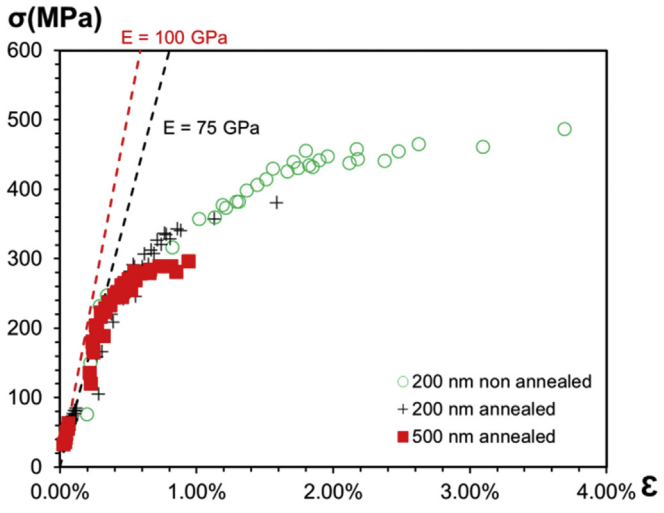

Fig. 2. Stress-strain curves obtained with the on-chip test structures for 200 nm and 500 nm specimen thicknesses. The annealing temperature is equal to 150 °C.

deformation of the annealed 500 nm thick sample was measured after release during 50 h. Then, it was left for 3200 h unattended under vacuum, and measured again.

The activation volume and the strain rate sensitivity exponent are defined respectively as:

$$V_{act} = M\, k_B\, T \left(\frac{\partial \ln \dot{\varepsilon}_p}{\partial \sigma}\right)_T, \tag{2}$$

$$m = \left(\frac{\partial \ln \sigma}{\partial \ln \dot{\varepsilon}_p}\right)_T = \frac{M k_B T}{\sigma V_{act}}, \tag{3}$$

where M is the Taylor factor, k_B is the Boltzmann constant, T is the temperature during the experiment, $\dot{\varepsilon}_p$ is the plastic strain rate, and σ is the applied stress. M is usually taken as equal to $\sqrt{3}$ for a textured thin film [30,31] while other authors use 3.06 [32,33] as for a FCC randomly textured polycrystal. No choice has been made in the following and the activation volume is thus plotted with unit Mb^3 in Fig. 5a, for the three types of films as a function of the initial plastic strain at which relaxation starts.

The logarithmic dependence of strain with time leads to a constant activation volume during stress relaxation [34]. The strain rate sensitivity exponent can then be deduced from Eq. (4) from the value of the activation volume. The strain rate sensitivity m shown in Fig. 5b as a function of the initial plastic strain is calculated from the stress measured at the beginning of the relaxation.

The activation volume decreases with increasing initial plastic deformation. Thus, the higher the initial dislocation density is, the lower is the activation volume which is consistent with the Cottrell-Stokes law for a thermally activated dislocation motion based

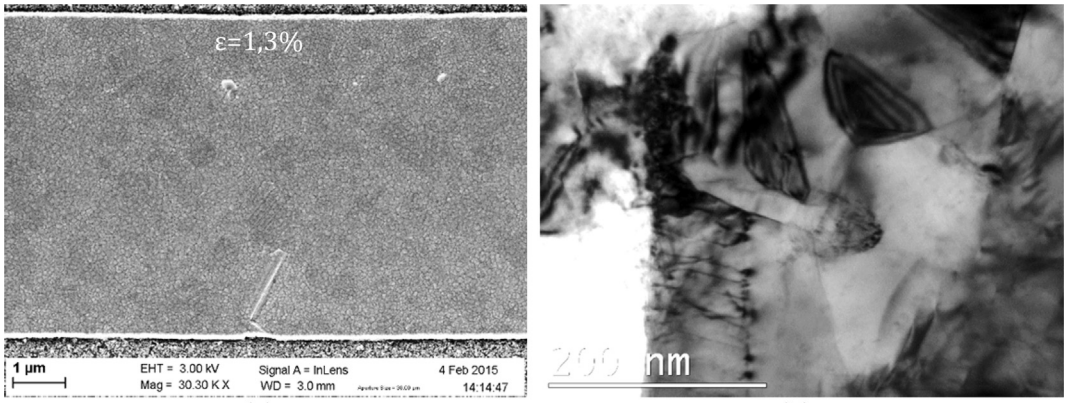

Fig. 3. a) Slip bands at the surface of the annealed 200 nm thick film, b) dislocation pile-up in an annealed 200 nm thick specimen after failure.

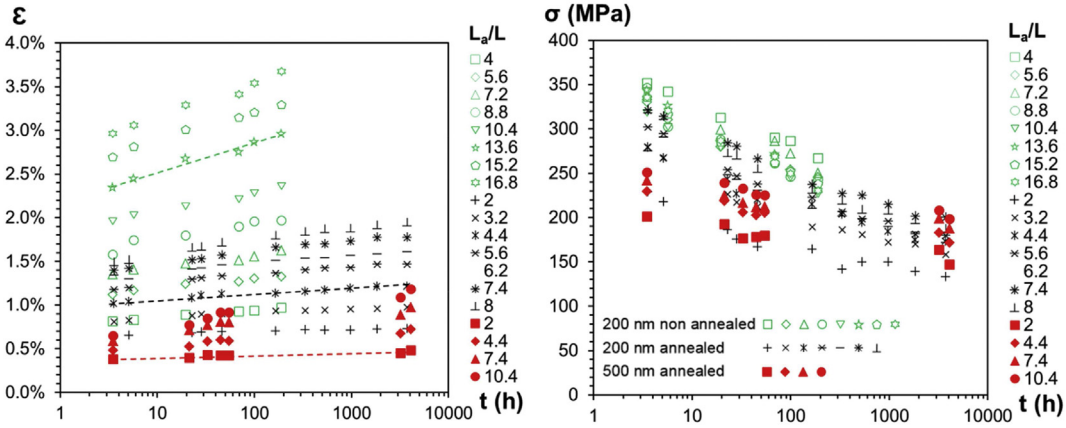

Fig. 4. Strain and stress change in different specimens. The parameter La/L is the ratio between the actuator length and the specimen length for one test structure. Each symbol represents a different test structure from the same series of specimens.

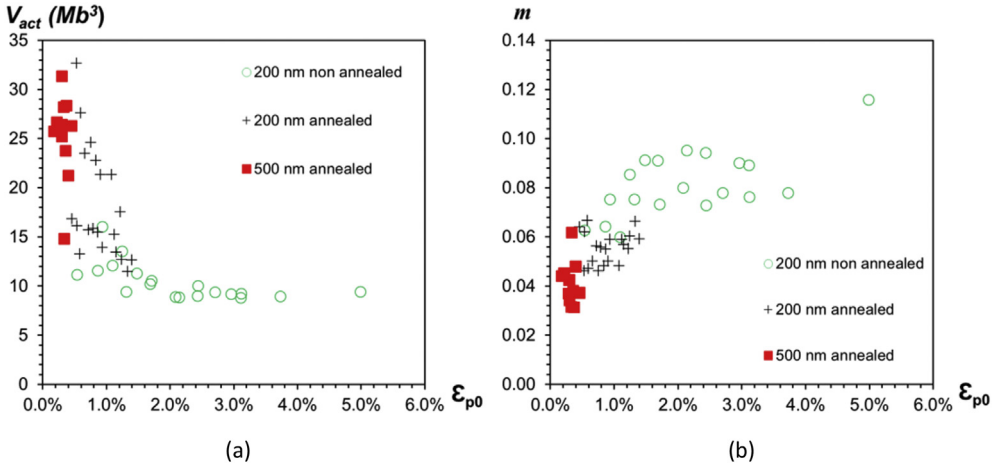

Fig. 5. Variation of (a) the activation volume V_{act} and (b) the strain rate sensitivity exponent m for the 200 (annealed and not annealed) and 500 nm films as a function of the initial plastic deformation (ε_{p0}).

deformation mechanism controlled by the inter-dislocation spacing [35].

The strain rate sensitivity exponent varies from 0.03 to about 0.1. These values are relatively high when compared to bulk Cu ($m < 0.01$) [36,37] but agree with values commonly measured for FCC ultrafine grain metals [38,39].

Fig. 6 a and b compare the typical fracture surface of a specimen which failed just after release, hence under moderate strain rates, with the one of a specimen which failed during relaxation, hence under extremely slow strain rates ($<10^{-7}$ s^{-1}). Under moderate strain rates, the fracture surfaces exhibit an intragranular failure mode whereas, under slow strain rates, failure appears mainly intergranular. Moreover during stress relaxation, the localization of plastic deformation inside large grains is not observed anymore. This change of failure mechanism is an indication of a change of deformation mechanism. As observed by Vayrette et al. [21] on self-actuated Cu structures, the deformation at slow strain rates remains homogeneous with an accumulation of defects at the grain boundaries.

Fig. 6c shows the surface of an annealed specimen after more than 3200 h of relaxation. After a long relaxation time, steps appear on the surface of the most highly deformed specimens. This may

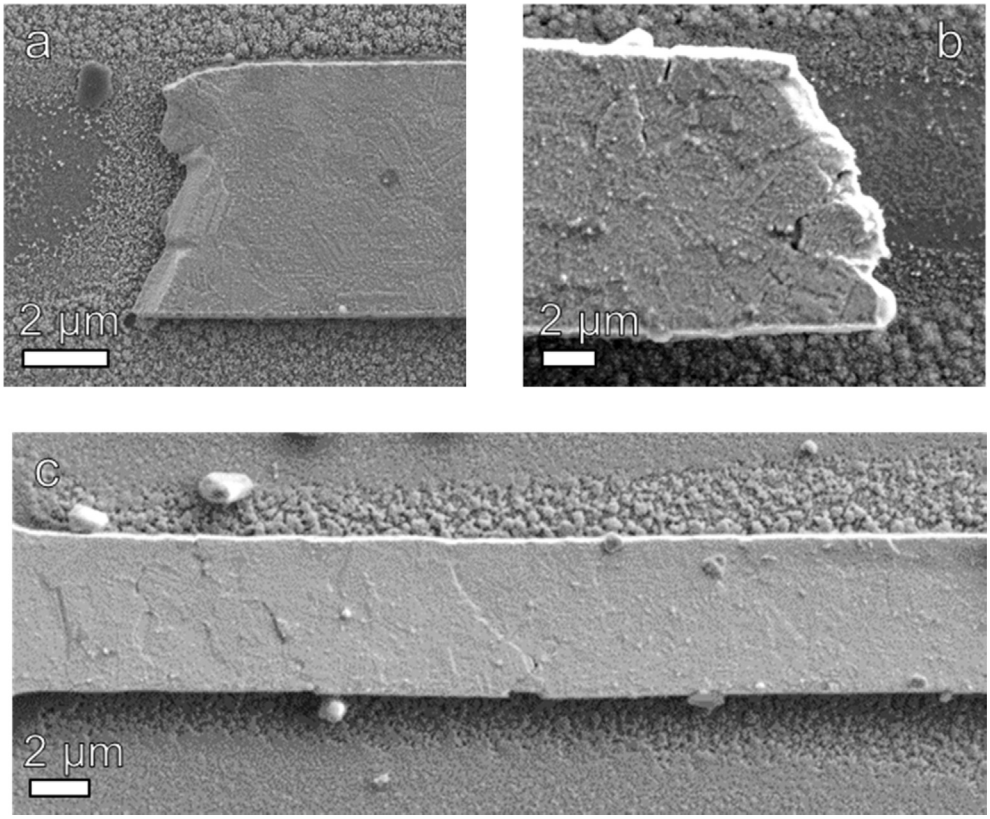

Fig. 6. Fracture surfaces of annealed 500 nm thick specimen with the failure occurring (a) just after the release, i.e. at moderate strain rate, or (b) under extremely low strain rate. (c) Surface of a 500 nm thick specimen 3200 h after release and deformed up to 3.2%.

indicate the occurrence of grain boundary sliding. On Fig. 6c, the 500 nm thick specimen is deformed up to 3.2% which is three times the maximum value measured before the onset of necking, see Fig. 2.

3.2. Irradiated copper films

One annealed 200 nm thick sample (involving thus a large number of elementary test structures) was irradiated, at room temperature, before release. On one set of test structures, the actuators have been left unirradiated while the specimens have been fully irradiated up to 1 dpa thanks to the masking device described in Ref. [17]. Another set of structures, fully protected from irradiation, is also available on the same sample. This set is referred to as the "reference set" in the following. For the irradiated specimens, the mismatch strain was not measured and was taken as equal to the one of the unirradiated material.

Fig. 7 presents the stress-strain response of several test specimens under irradiated and non-irradiated conditions. The strength of the irradiated test structures increases by almost a factor 2 compared to the reference specimens, which corresponds to an irradiation hardening between 100 and 150 MPa. The irradiated structures show a significant relaxation/creep response as well.

The activation volumes and rate sensitivity exponents are extracted from the strain versus time evolution (Fig. 7b) with the same method as for the unirradiated material assuming a logarithmic variation. The two parameters are similar in the irradiated and in the control sets, as shown in Fig. 8. The same deformation mechanisms probably take place in both conditions. Moreover, SEM observations do not show any qualitative differences of surface appearance between the two sets of test specimen regardless whether the observation is made right after release or after a long relaxation time.

Fig. 9 compares the initial plastic strain rate in the two sets of test structures measured at the beginning of the relaxation. Even if the deformation mechanisms remain the same after irradiation, the plastic strain rates in the irradiated specimens set are smaller than what would be expected in the same conditions on unirradiated specimens at the same stress level. This is consistent with the significant hardening observed on the stress-strain curves.

3.3. Cu films deformed under irradiation

In order to assess the irradiation creep behavior, the release is performed before irradiation. In this way, the irradiation is performed on the specimen beams *in situ* under an applied stress. The variation of the strain can be monitored from the measurements of the displacement in a SEM before and after an irradiation event. Multiple irradiation steps were performed up to a total dose of 8 dpa while fully protecting the actuators. The specimen length before deformation is equal to 50 μm. On the first and second irradiation steps, a small margin has been taken to ensure that the actuator remained fully protected and so the specimens were only partially irradiated. The boundary between the irradiated and unirradiated area can be clearly seen on the SEM images and can thus be accurately defined. By assuming that only the irradiated part of the specimen deforms during the irradiation (an assumption that will be justified later) we can calculate the strain of the irradiated part from the total specimen by multiplying the measured total strain with the ratio between the total length and the irradiated length of the specimen. However, for the second irradiation step, the irradiated length is very small and the increase in strain is within the experimental uncertainty. Hence, the points corresponding to this step have not been taken into account in the analysis of the strain rate under irradiation.

For the last three irradiation steps, the masking device has been very accurately positioned in order to fully irradiate the specimen beams. No correction is required for these data.

The sample was irradiated after more than 3200 h of stress relaxation at room temperature out of flux. The strain rate of the unirradiated material is thus negligible during the duration of the experiment (involving several irradiations) which lasts for about a few tens of hours. Fig. 10 shows the evolution of the stress applied to the test beam and of the additional plastic deformation created under irradiation, ε_{irr}, with the increase in dose. We can note in Fig. 10 a) that the relaxation of the irradiated material during the 12 h nighttime between two irradiation steps is negligible compared to the relaxation during irradiation. This validates the assumption made above that the viscoplastic relaxation of both unirradiated and irradiated specimens (as addressed in Figs. 4 and 7) is negligible during the experiment compared to the irradiation creep contribution.

The strain rate under irradiation can be approximately determined by the slope between each two data points in the plastic strain versus time evolution. Fig. 11 shows the variation of the strain variation with dose as a function of the mean value of the stress between the two points, following a power law with stress. If we assume a linear dependence between the strain rate and the

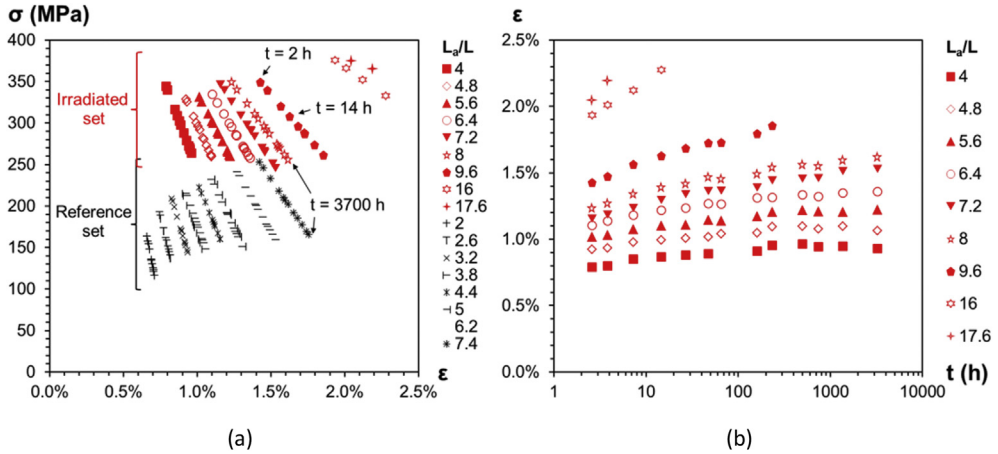

Fig. 7. (a) Stress-strain evolution with time for annealed 200 nm thick samples either irradiated or non irradiated. (b) Variation of strain with time for the irradiated specimens. The parameter *La/L* is the ratio between the actuator length and the specimen length for one test structure. Each value represents a different test structure from the same series of test specimens.

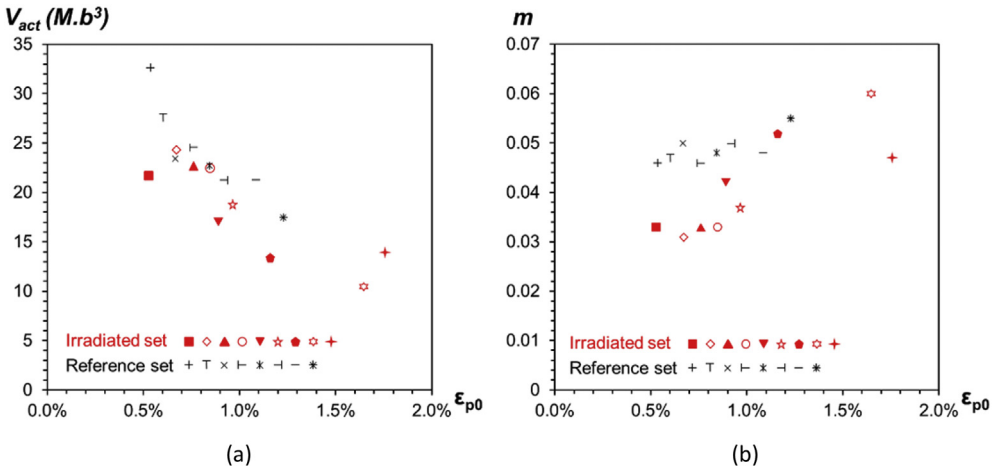

Fig. 8. Variation of the (a) activation volume V_{act} and (b) strain rate sensitivity exponent m as a function of the plastic pre-strain in the irradiated and unirradiated specimens (ε_{p0}).

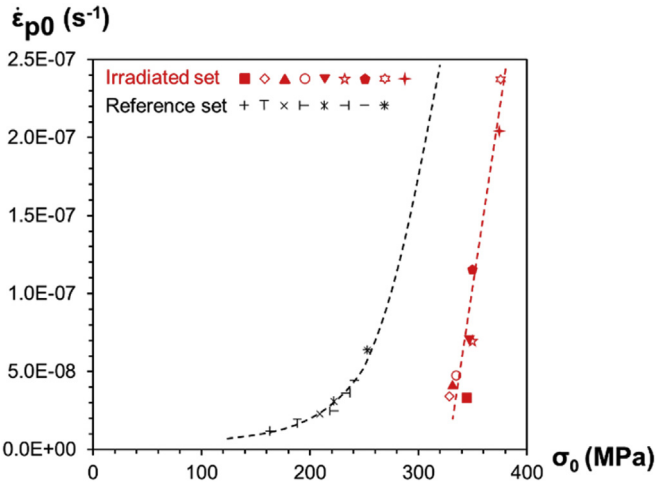

Fig. 9. Initial plastic strain rate in the irradiated and control sets of test structures.

damage rate, φ (in dpa/s), which is the usual relationship promoted in the literature [40,41], one finds:

$$\dot{\varepsilon}_{irr} = K\varphi\sigma^5, \tag{4}$$

where K is equal to 2.2×10^{-14} dpa^{-1} MPa^{-5}.

The strain rate sensitivity exponent m is constant and equal to $1/5 = 0.2$ under irradiation and the corresponding activation volume varies from 12 Mb^3 at 100 MPa to 6 Mb^3 at 250 MPa which is slightly lower than out of the ion flux.

The SEM observations do not reveal any detectable change of the specimen surface after the different irradiation steps. The deformed specimens appear homogenous along the entire beam length without any visible plastic localization and in particular no slip trace is observed after irradiation creep. EBSD analyses do not reveal any grain growth after irradiation when compared to the reference set.

TEM samples have been extracted in several specimen beams by FIB milling. Fig. 12 shows, on a TEM micrograph, evidence of dislocations pinned at obstacles with the presence of several jogs. This is not observed in the reference samples where the dislocation lines show a uniform curvature as in Fig. 3b). Given that the deformation out of flux is negligible, the dislocation pinning mechanism must thus occur under irradiation.

4. Discussion

4.1. Non irradiated behavior

Under moderate strain rates, marked plastic localization is observed in large grains whithin the gauge section of the

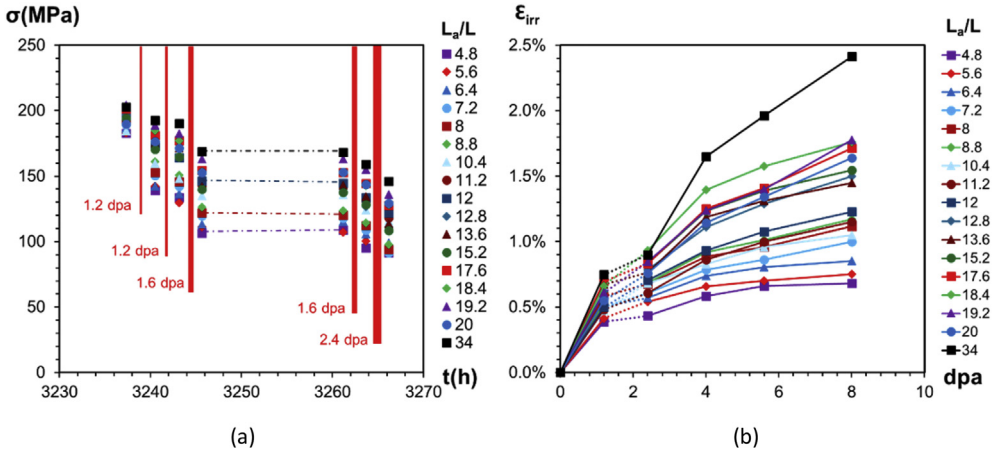

Fig. 10. (a) Stress versus time evolution after each irradiation step and (b) plastic strain produced under irradiation versus irradiation damage quantified in dpa.

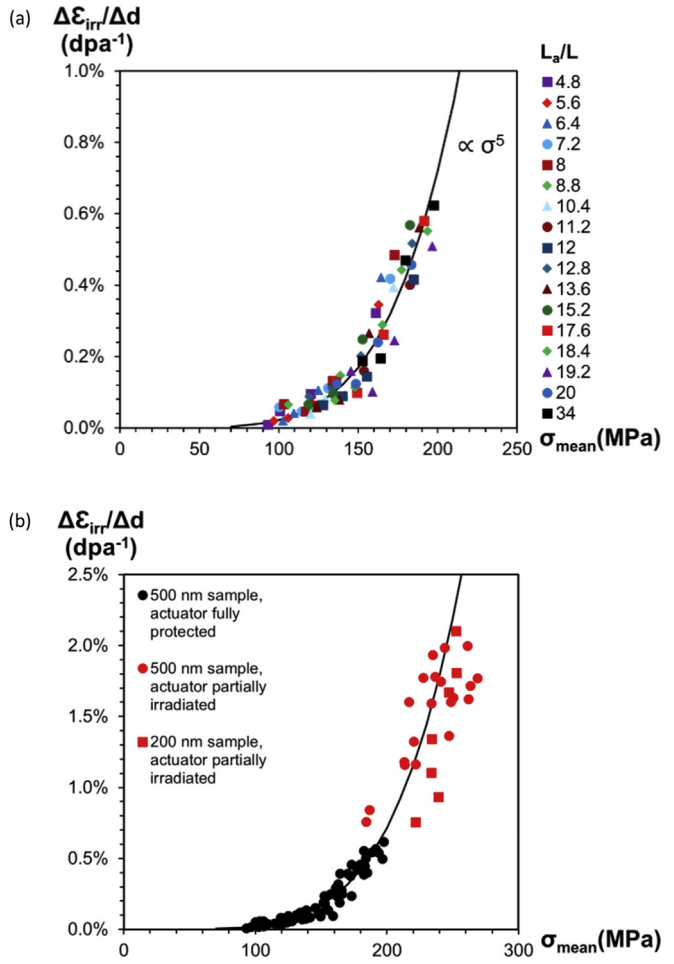

Fig. 11. (a) Plastic strain rate (relative to the dose) under irradiation versus the mean applied stress under irradiation. (b) Comparison between the strain rates developing in different types of specimens tested with the on-chip method. The solid line indicates the power creep law in σ^5.

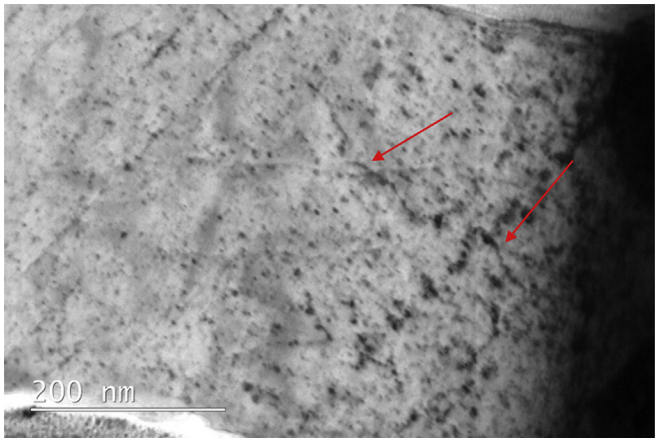

Fig. 12. TEM micrograph of a specimen beam deformed by creep under irradiation, showing evidences of jogged dislocations (see arrows).

specimens. Both SEM and TEM observations show evidences that deformation is controlled by dislocation glide, involving intense slip bands emerging on the surface and dislocation pile-ups.

On the other hand, a change in the deformation mechanism occurs at much slower strain rates ($<10^{-7}$ s^{-1}). The deformation of the specimen appears to be more homogenous and can reach values significantly larger than at higher strain rates. Part of the plastic deformation probably occurs by grain boundary sliding. Nevertheless, the strain rate sensitivity exponent is too low compared to the theoretical value of $m = 0.5$ [42] for this mechanism to be predominant. In the same way, mechanisms such as Coble creep, $m = 1$ [43] or other diffusive processes where $V_{act} \sim 1\ b^3$ can be excluded. This change of mechanism was already observed in nanocrystalline Cu bulk materials [44,45] and on similar Cu films [21].

The activation volume decreases for increasing initial plastic deformation. This is consistent with a dependence of the activation volume with dislocation density. Actually, the usual Cottrell-Stokes law [46] states that the activation volume is inversely proportional to the flow stress which is, in turn, inversely proportional to the spacing between dislocations. Hence, with this law, the higher the dislocation density is, the lower is the activation volume. This observation is also consistent with the slower *post* irradiation relaxation. The SFT created by irradiation behave as obstacles for dislocation motion, slowing down the relaxation rate. It also explains the significant hardening measured after irradiation. Consequently, there are good reasons to claim that the deformation remains controlled by dislocation glide in these conditions.

4.2. Irradiation creep

Under irradiation, the strain rate is several orders of magnitude larger than what is observed out of flux in the unirradiated or irradiated materials. It has been shown in Ref. [17], using a basic thermal model, that specimen heating due to the ion flux is negligible in the present test conditions. Moreover, no cavities have been observed by TEM, and the volume increase due to ion implantation is much too small to explain the observed deformation. A classical high temperature deformation mechanism or an additional swelling of the specimen can thus be excluded. Hence, the origin of the significant deformation produced under the ion flux must be related to a room temperature creep phenomenon induced by irradiation.

The validity and the reproducibility of the power law relationship found under irradiation have been checked out with two other complementary experiments using two different sets of specimens: one involving 500 nm thick annealed Cu films and a second involving 200 nm thick annealed Cu films. The geometries of the specimens are similar to the ones reported before for the tests under irradiation but the stress applied to the specimens are higher before irradiation. The irradiation is also conducted with similar conditions, *i.e.* at room temperature, with an ion energy of 600 keV or 1200 keV and a flux around 5×10^{-4} dpa s^{-1}. A single irradiation step at 0.26 dpa is performed on both samples. However, contrary to the previous 500 nm sample used for the irradiation creep, the actuators in both samples are partially irradiated (a few tens of micrometers on several hundred micrometer actuators) during the experiments which lead to a slight overestimation of the stress in the specimen due to the stress relaxation under irradiation in the actuator. However, the dose is sufficiently low and the actuators long enough to consider that the stress relaxation in the actuator remains low.

Fig. 11b compares the strain rates extracted from the three experiments under irradiation as a function of an average of the stress measured before and after each irradiation step. The samples with the partially irradiated actuator give results in good agreement with the power law found previously. The power law with an exponent 5 is valid for the 500 nm thick films undergoing between 100 and 250 MPa stress under irradiation. The identified creep law

works well for the 200 nm thick specimens as well, which suggests that the observed irradiation creep depends only weakly on the thickness. Besides, since the grain size is directly related to the specimen thickness in the annealed state (the in-plane grain size is close to the thickness of the film), the creep behavior of the copper films does not significantly depend on grain size, at least in this range of submicron grain size.

In Ref. [17], we reported a saturation of the irradiation creep phenomenon after 1.6 dpa. This saturation was in reality an artefact caused by a problem occurring during the transport of the samples. Parts of the actuators were sticking to the substrate due to a contact with the protection used during the travelling in between the two testing facilities. This resulted in a decrease of the effective length of the actuator, with only the freestanding part between the point of adhesion zone and the specimen still pulling on the specimen. The stress relaxation accompanying the deformation of the specimen was thus incorrectly evaluated at larger dose in Ref. [17] because of a wrong estimation of the stress applied to the specimens. This issue has been solved to produce the results presented in this paper.

Few experiments can be found in the literature on the creep behavior of pure Cu under irradiation. The experiments conducted by Aitkhozhin et al. [47,48] lead also to a power creep law with an exponent equal to 5 for Cu samples undergoing a neutron flux at temperatures between 150 °C and 500 °C, and applied stress ranging between 20 and 65 MPa. Jung at al [49,50] reported, for irradiation with protons at 150 °C, a transition from a linear regime below 50 MPa to a power law regime at higher stress. These two studies are thus fully consistent with the results described here. This also indicates that the Cu films tested in this work can be considered as representative of the bulk material behavior regarding the irradiation creep mechanisms in agreement also with the lack of dependence on grain size mentioned above. This is a very important element of assessment for the proposed methodology. A study with heavy ions has been recently published by Tai et al. [15], based on bulge tests on Cu membranes. A linear creep behavior under irradiation at 200 °C below a stress of 10 MPa was observed with negligible creep at room temperature under the same irradiation parameters and applied stress. This last result is also consistent with our study since the strain rate at 10 MPa should be around the extremely low value of 2×10^{-9} dpa^{-1} if the power law creep still holds at low stress.

4.3. Physical mechanism of irradiation creep in Cu

A large stress exponent (larger than the so called “natural exponent“ of 3) is frequently observed in materials creep. In the case of irradiation creep of copper, the physical meaning of the power law regime has been explained by Jung [50] and Aitkhozkin [47] as resulting from climb assisted glide of dislocations. Indeed, the ion flux leads to the creation of point defects that are absorbed by dislocations allowing the unpinning by climb. After the climb event, the dislocation can glide again. A similar mechanism is also used to explain the power law with an exponent 5 creep behavior of Cu at high temperature [51]. The *post mortem* TEM observations, see Fig. 12, indicate indeed the activation of dislocation glide in a field of obstacles made of irradiation defects such as SFT.

The SEM observations of the specimen surface do not show any significant localization of the plastic deformation during relaxation under irradiation. The deformation appears very homogenous. Large deformation, when compared to the values reached under static loading, accumulates during creep without necking of the specimen. Moreover, failure is never observed under irradiation. This point is consistent with the high value of the rate sensitivity exponent m which is known to delay plastic localization [52]. This absence of necking implies deformation mechanisms which are highly viscoplastic with low activation volume consistent with the measured data.

The concentration of vacancies and interstitials can be calculated from the standard rate theory [53] by considering the balance between the production and loss rates of point defects under irradiation. The loss of point defects occurs either by recombination between vacancies and interstitials, by clustering of point defects or by annihilation at sinks such as dislocations and grain boundaries. The sink strength is highly dependent on the sink geometry and on the sink density [54]. Hence, the calculated flux of point defects towards a sink, such as a dislocation, is very much dependent on the microstructure of the material.

However, it has been observed that the temperature dependence of irradiation creep is very low, besides, the experiments have shown that the same power creep law is appropriate for every specimen, independently of the plastic deformation accumulated before irradiation (which varied between ~0.2% and ~3%). Even the specimens which started the necking process before irradiation behave in a way similar to the slightly deformed specimens. Moreover, the creep law still remains the same for different thicknesses and therefore different grain sizes. Thus, the power law creep does not significantly depend on the microstructure of the films (dislocation density and grain size), at least in the range of microstructure sizes addressed in the present study. This is also supported by the good adequacy with literature results on bulk Cu, see above.

Therefore, if the deformation mechanism involves climb-assisted glide of dislocations (as suggested by the power law) the climb event is not the result of point defect flux over long distances as predicted by the rate theory, which would then highly depend on the microstructure and temperature. In order to explain these features, one is led to admit that, most probably, the climb event is the result of displacement cascades occurring in the vicinity of dislocations. This is in agreement with the predictions of Voskoboinikov [55,56] based on molecular dynamics calculations.

For dislocation assisted creep, the creep rate $\dot{\varepsilon}$ can be calculated from the density of mobile dislocations, ρ, the Burgers vector, b, and the dislocation velocity, v, using the Orowan equation:

$$\dot{\varepsilon} = \rho\, b\, v. \tag{5}$$

The density of mobile dislocations ρ is proportional, according to Taylor's law, to σ^2:

$$\rho = \alpha\left(\frac{\sigma}{Gb}\right)^2, \tag{6}$$

with G the shear modulus and α a material constant.

In a climb-assisted glide model, the deformation comes from the distance d a dislocation can glide after climbing before being pinned again. The kinetics is prescribed by the duration t_w a mobile dislocation has to wait to climb and overcome the obstacle. Hence, the dislocation velocity can be written $v = \frac{d}{t_w}$.

The distance d the dislocation can glide after overcoming an obstacle is likely to be given by the distance to the neighboring obstacle.

The inverse of the duration t_w is directly proportional to the flux of point defects which are efficient in inducing dislocation climb. Two extreme hypotheses are possible: either any site along the dislocation, with a capture radius r, is efficient in absorbing defects, or alternatively only sites with geometrical jogs imposed by the curvature are efficient. The proportion of irradiated volume which leads to “efficient point defects” is therefore ρr^2 in the first case and $\rho r^3 x$ in the second case where x is the number of jogs per unit length. Geometrically, x will be related to the curvature $1/R$ which

itself is proportional to σ because of the equilibrium of the curved dislocation under an applied stress. Since the dislocation density ρ brings a σ^2 dependence, the velocity will give an exponent in stress of 2–3 and the strain rate will depend on the stress with a power 4 or 5. Accordingly the strain rate is expected to be linear with the irradiation flux φ, essentially independent of the temperature and the microstructure. Hence we find, with the second hypothesis, $\dot{\varepsilon} \propto \varphi\sigma^5$.

This simple model, although not yet quantitative due to the difficulty of assessing the efficiency of dislocation cascades in the vicinity of a jog on a dislocation, provides an additional confidence in the physical scenario elaborated in this discussion. It also indicates that the specificities of the thin film geometry, i.e. the free surfaces and the small grain size do not significantly affect our result, at least within the investigated range of thicknesses and grain sizes, which in turns explains the surprisingly good comparison with bulk specimens.

5. Conclusion

The deformation of submicron thick Cu films under irradiation has been studied using an on chip test method, supplemented by electron microscopy characterizations and compared to the response out of flux. The main conclusions are the following:

- Under moderate strain rate out of the ion flux, the plastic deformation is localized in large grains with evidences of numerous intense slip bands. Failure occurs mainly by intragranular cracking.
- At extremely slow creep-type strain rate ($<10^{-7}$ s^{-1}) out of the ion flux, the deformation of the specimens is homogenous and can exceed a few percents. No new slip band develops on the surface. The magnitude of the activation volume suggests that the deformation remains controlled by dislocation glide but a component of grain boundary sliding can potentially be present.
- The irradiated specimens deformed out of flux show a behavior similar to the unirradiated ones with the same activation volume. However, the presence of stacking fault tetrahedra leads to significant hardening and to a lower strain rate for the same applied stress.
- Under irradiation, the strain rate is several orders of magnitude higher than its value out of flux. Moreover, large additional plastic deformation of several percents can accumulate without any plastic localization. The strain rate follows a creep power law with a stress exponent equal to 5. This relationship can be explained and theoretically justified by a mechanism of climb assisted glide of dislocations. The displacement cascades induced by ion bombardment lead to a uniform probability of climb events allowing the unpinning of dislocations. This results in a highly viscoplastic behavior leading to relatively fast creep and preventing the occurrence of necking.

This work demonstrates the ability of the on-chip method to study irradiation creep in model materials. In the perspectives, the method will be applied to more complex metallic alloys and the coupling with TEM *in situ* characterization based on the on chip test platform [34] should allow a deeper understanding of the physical mechanisms at the origin of the irradiation creep.

Acknowledgements

The authors are thankful to R. Vayrette for the help provided in clean room at UCL and C. Bachelet, J. Bourçois and S. Picard for the assistance during the irradiation experiments on the ARAMIS facility at CSNSM/IN2P3/CNRS in Orsay. J-P Raskin and T. Pardoen also acknowledge the support of the Belgian Science Policy through the IAP 7/21 project.

References

[1] S.T. Konobeevsky, N.F. Pravdynk, V.I. Kutaitsev, A/CONF. 8, in: First International Conference on Peaceful Uses of Atomic Energy, Geneva, 1955, p. 681.
[2] A.C. Roberts, A.H. Cottrell, LXXII. Creep of alpha uranium during irradiation with neutrons, Philos. Mag. 1 (1956) 711–717.
[3] V. Fidleris, The irradiation creep and growth phenomena, J. Nucl. Mater. 159 (1988) 22–42.
[4] Y. Ashkenazy, R.S. Averback, Irradiation induced grain boundary flow—a new creep mechanism at the nanoscale, Nano Lett. 12 (2012) 4084–4089.
[5] C. Xu, G.S. Was, In situ proton irradiation creep of ferritic–martensitic steel T91, J. Nucl. Mater. 441 (2013) 681–687.
[6] R.V. Hesketh, A possible mechanism of irradiation creep and its reference to uranium, Philos. Mag. 7 (1962) 1417–1420.
[7] P.T. Heald, M.V. Speight, Steady-state irradiation creep, Philos. Mag. 29 (1974) 1075–1080.
[8] J.H. Gittus, Theory of dislocation creep for a material subjected to bombardment by energetic particles role of thermal diffusion, Philos. Mag. 30 (1974) 751–764.
[9] D.G. Franklin, G.E. Lucas, A.L. Bement, Creep of Zirconium Alloys in Nuclear Reactors, ASTM STP 815, 1983.
[10] P. Morize, J. Baicry, J. Mardon, Effect of Irradiation at 588 K on Mechanical Properties and Deformation Behavior of Zirconium Alloy Strip, ASTM STP 939, 1987.
[11] M.L. Grossbeck, L.K. Mansur, M.P. Tanaka, Irradiation Creep in Austenitic Stainless Steels at 60 to 400°C with a Fusion Reactor Helium to dpa Ratio, ASTM STP 1046, 1989.
[12] J. Garnier, et al., Irradiation creep of SA 304L and CW 316 stainless steels: mechanical behaviour and microstructural aspects. Part I: experimental results, J. Nucl. Mater. 413 (2011) 63–69.
[13] P. Jung, A. Schwarz, H.K. Sahu, An apparatus for applying tensile, compressive and cyclic stresses on foil specimens during light ion irradiation, Nucl. Instrum. Methods Phys. Res. Sect. A 234 (1985) 331–334.
[14] Y. Serruys, et al., JANNUS: a multi-irradiation platform for experimental validation at the scale of the atomistic modelling, J. Nucl. Mater. 386–388 (2009) 967–970.
[15] K. Tai, R.S. Averback, P. Bellon, Y. Ashkenazy, Irradiation-induced creep in nanostructured Cu alloys, Scr. Mater. 65 (2011) 163–166.
[16] S. Özerinç, R.S. Averback, W.P. King, In situ creep measurements on micropillar samples during heavy ion irradiation, J. Nucl. Mater. 451 (2014) 104–110.
[17] P. Lapouge, F. Onimus, R. Vayrette, J.-P. Raskin, T. Pardoen, Y. Bréchet, A novel on chip test method to characterize the creep behavior of metallic layers under heavy ion irradiation, J. Nucl. Mater. 476 (2016) 20–29.
[18] A. Boé, A. Safi, M. Coulombier, T. Pardoen, J.-P. Raskin, Internal stress relaxation based method for elastic stiffness characterization of very thin films, Thin Solid Films 518 (2009) 260–264.
[19] G. Lemoine, L. Delannay, H. Idrissi, M.-S. Colla, T. Pardoen, Dislocation and back stress dominated viscoplasticity in freestanding sub-micron Pd films, Acta Mater. 111 (2016) 10–21.
[20] S. Gravier, et al., New on-chip nanomechanical testing laboratory - applications to aluminum and polysilicon thin films, J. Microelectromech. Syst. 18 (2009) 555–569.
[21] R. Vayrette, J.-P. Raskin, T. Pardoen, On-chip fracture testing of freestanding nanoscale materials, Eng. Fract. Mech. 150 (2015) 222–238.
[22] T. Pardoen, et al., A versatile lab-on-chip test platform to characterize elementary deformation mechanisms and electromechanical couplings in nanoscopic objects, Comptes Rendus Phys. 17 (2016) 485–495.
[23] M. Coulombier, G. Guisbiers, M.-S. Colla, R. Vayrette, J.-P. Raskin, T. Pardoen, On-chip stress relaxation testing method for freestanding thin film materials, Rev. Sci. Instrum. 83 (2012) 105004.
[24] D. Fabrègue, N. André, M. Coulombier, J.P. Raskin, T. Pardoen, Multipurpose nanomechanical testing machines revealing the size-dependent strength and high ductility of pure aluminium submicron films, Micro Nano Lett. 2 (2007) 13.
[25] A. Boé, A. Safi, M. Coulombier, D. Fabrègue, T. Pardoen, J.-P. Raskin, MEMS-based microstructures for nanomechanical characterization of thin films, Smart Mater. Struct. 18 (2009) 115018.
[26] J.F. Ziegler, J.P. Biersack, M.D. Ziegler, SRIM, the Stopping and Range of Ions in Matter, SRIM Co., Chester, Maryland, 2008.
[27] G.G. Stoney, The tension of metallic films deposited by electrolysis, Proc. R. Soc. Math. Phys. Eng. Sci. 82 (1909) 172–175.
[28] H. Huang, F. Spaepen, Tensile testing of free-standing Cu, Ag and Al thin films and Ag/Cu multilayers, Acta Mater. 48 (2000) 3261–3269.
[29] Material Property Database. [Online]. http://www.mit.edu/~6.777/matprops/copper.htm. (Accessed 29 July 2013).
[30] H. Conrad, Grain size dependence of the plastic deformation kinetics in Cu, Mater. Sci. Eng. A 341 (2003) 216–228.
[31] P. Wang, Y. Fu, G. Zhang, R. Ma, The grain growth and phase transformation in Ni thin films induced by ion irradiation, Vacuum 42 (1991) 995–999.

[32] D. Torre, E.V. Pereloma, C.H.J. Davies, Strain rate sensitivity and apparent activation volume measurements on equal channel angular extruded Cu processed by one to twelve passes, Scr. Mater. 51 (2004) 367–371.
[33] R.K. Guduru, K.L. Murty, K.M. Youssef, R.O. Scattergood, C.C. Koch, Mechanical behavior of nanocrystalline copper, Mater. Sci. Eng. A 463 (2007) 14–21.
[34] M.-S. Colla, et al., Dislocation-mediated relaxation in nanograined columnar palladium films revealed by on-chip time-resolved HRTEM testing, Nat. Commun. 6 (2015) 5922.
[35] A.H. Cottrell, R.J. Stokes, Effects of temperature on the plastic properties of aluminium crystals, Proc. R. Soc. Math. Phys. Eng. Sci. 233 (1955) 17–34.
[36] P.S. Follansbee, U.F. Kocks, A constitutive description of the deformation of copper based on the use of the mechanical threshold stress as an internal state variable, Acta Metall. 36 (1988) 81–93.
[37] R.P. Carreker, W.R. Hibbard, Tensile deformation of high-purity copper as a function of temperature, strain rate, and grain size, Acta Metall. 1 (1953) 654–663.
[38] I.-C. Choi, Y.-J. Kim, Y.M. Wang, U. Ramamurty, J. Jang, Nanoindentation behavior of nanotwinned Cu: influence of indenter angle on hardness, strain rate sensitivity and activation volume, Acta Mater. 61 (2013) 7313–7323.
[39] A. Pineau, A. Amine Benzerga, T. Pardoen, Failure of metals III: fracture and fatigue of nanostructured metallic materials, Acta Mater. 107 (2016) 508–544.
[40] J.R. Matthews, M.W. Finnis, Irradiation creep models — an overview, J. Nucl. Mater. 159 (1988) 257–285.
[41] J. Chen, P. Jung, W. Hoffelner, Irradiation creep of candidate materials for advanced nuclear plants, J. Nucl. Mater. 441 (2013) 688–694.
[42] Y. Wang, A. Hamza, E. Ma, Temperature-dependent strain rate sensitivity and activation volume of nanocrystalline Ni, Acta Mater. 54 (2006) 2715–2726.
[43] S. Cheng, E. Ma, Y. Wang, L. Kecskes, K. Youssef, C. Koch, U. Trociewitz, K. Han, Tensile properties of in situ consolidated nanocrystalline Cu, Acta Mater. 53 (2005) 1521–1533.
[44] Z. Jiang, H. Zhang, C. Gu, Q. Jiang, J. Lian, Deformation mechanism transition caused by strain rate in a pulse electric brush-plated nanocrystalline Cu, J. Appl. Phys. 104 (2008) 053505.
[45] J.J. Hu, X.P. Zhang, G.X. Sun, G.Y. Wang, Deformation mechanism of an electric brush-plated nanocrystalline Cu investigated by tensile testing and nano-indentation creep, Mater. Res. Innov. 19 (2015) S181–S186.
[46] C. Duhamel, Y. Brechet, Y. Champion, Activation volume and deviation from Cottrell–Stokes law at small grain size, Int. J. Plast. 26 (2010) 747–757.
[47] E.S. Aitkhozhin, E.V. Chumakov, Radiation-induced creep of copper, aluminium and their alloys, J. Nucl. Mater. 233–237 (1996) 537–541.
[48] S. Ibragimov, E.S. Aitkhozhin, Y.S. Pyatiletov, Radiation-induced Creep of Aluminium and Copper, ASTM STP 956, 1987.
[49] P. Jung, Irradiation creep of 20% cold-worked copper, J. Nucl. Mater. 200 (1993) 138–140.
[50] P. Jung, M.I. Ansari, A correlation between irradiation creep strength and yield stress of FCC metals and alloys, J. Nucl. Mater. 138 (1986) 40–45.
[51] M.E. Kassner, M.-T. Pérez-Prado, Five-power-law creep in single phase metals and alloys, Prog. Mater. Sci. 45 (2000) 1–102.
[52] J.W. Hutchinson, K.W. Neale, Influence of strain-rate sensitivity on necking under uniaxial tension, Acta Metall. 25 (1977) 839–846.
[53] G.S. Was, Fundamentals of Radiation Materials Science: metals and Alloys, Springer, New York, 2007.
[54] R. Bullough, M.R. Hayns, M.H. Wood, Sink strengths for thin film surfaces and grain boundaries, J. Nucl. Mater. 90 (1980) 44–59.
[55] R.E. Voskoboinikov, MD simulations of collision cascades in the vicinity of a screw dislocation in aluminium, Nucl. Instrum. Methods Phys. Res. Sect. B Beam Interact. Mater. At. 303 (2013) 104–107.
[56] R.E. Voskoboinikov, Interaction of collision cascades with an isolated edge dislocation in aluminium, Nucl. Instrum. Methods Phys. Res. Sect. B Beam Interact. Mater. At. 303 (2013) 125–128.